PCCP

ROYAL SOCIETY OF CHEMISTRY

PAPER

View Article Online
View Journal | View Issue

Cite this: *Phys. Chem. Chem. Phys.*, 2023, **25**, 5592

Relativistic quantum calculations to understand the contribution of f-type atomic orbitals and chemical bonding of actinides with organic ligands†

Andy D. Zapata-Escobar,[a] Srimanta Pakhira,[b] Joaquin Barroso-Flores,[c] Gustavo A. Aucar*[ad] and Jose L. Mendoza-Cortes ‡*[ef]

The nuclear waste problem is one of the main interests of rare earth and actinide element chemistry. Studies of actinide-containing compounds are at the frontier of the applications of current theoretical methods due to the need to consider relativistic effects and approximations to the Dirac equation in them. Here, we employ four-component relativistic quantum calculations and scalar approximations to understand the contribution of f-type atomic orbitals in the chemical bonding of actinides (Ac) to organic ligands. We studied the relativistic quantum structure of an isostructural family made of Plutonium (Pu), Americium (Am), Californium (Cf), and Berkelium (Bk) atoms with the redox-active model ligand DOPO (2,4,6,8-tetra-*tert*-butyl-1-oxo-1*H*-phenoxazin-9-olate). Crystallographic structures were available to validate our calculations for all mentioned elements except for Cf. In short, state-of-the-art relativistic calculations were performed at different levels of theory to investigate the influence of relativistic and electron correlation effects on geometrical structures and bonding energies of Ac-$DOPO_3$ complexes (Ac = Pu, Am, Cf, and Bk): (1) the scalar (sc) and spin–orbit (so) relativistic zeroth order regular approximation (ZORA) within the hybrid density functional theory (DFT) and (2) the four-component Dirac equation with both the Dirac–Hartree–Fock (4c-DHF) and Lévy–Leblond (LL) Hamiltonians. We show that sr- and so-ZORA-DFT could be used as efficient theoretical models to first approximate the geometry and electronic properties of actinides which are difficult to synthesize or characterize, but knowing that the higher levels of theory, like the 4c-DHF, give closer results to experiments. We also performed spin-free 4c calculations of geometric parameters for the Americium and Berkelium compounds. To the best of our knowledge, this is the first time that these kinds of large actinide compounds (the largest contains 67 atoms and 421 electrons) have been studied with highly accurate four-component methods (all-electron calculations with 6131 basis functions for the largest compound). We show that relativistic effects play a key role in the contribution of f-type atomic orbitals to the frontier orbitals of *Ac*-$DOPO_3$ complexes. The analysis of the results obtained applying different theoretical schemes to calculate bonding energies is also given.

Received 18th November 2022,
Accepted 10th January 2023

DOI: 10.1039/d2cp05399c

rsc.li/pccp

[a] *Institute of Modelling and Innovation on Technology (IMIT), CONICET-UNNE, Argentina*
[b] *Department of Physics, Department of Metallurgy Engineering and Materials Science (MEMS), Centre for Advanced Electronics (CAE), Indian Institute of Technology Indore (IIT Indore), Simrol, Khandwa Road, Indore, 453552, Madhya Pradesh (M.P.), India*
[c] *Instituto de Química, Universidad Nacional Autónoma de México (UNAM), Circuito Exterior SN, Ciudad Universitaria, Coyoacán CP, 04510 Ciudad de Mexico, Mexico*
[d] *Physics Department, Natural and Exact Science Faculty, Northeastern University of Argentina, Argentina. E-mail: gaaucar@conicet.gov.ar*
[e] *Department of Physics, Scientific Computing, Material Sciences and Engineering, High-Performance Material Institute, Condensed Matter-High Magnetic Field National Lab, Florida State University, Tallahassee, FL, 32310, USA*
[f] *Department of Chemical and Biomedical Engineering, FAMU-FSU Joint College of Engineering, Tallahassee, FL 32310, USA*

† Electronic supplementary information (ESI) available: The equilibrium geometries with the *x*, *y*, *z* coordinators using the scalar (ZORA) and the 4-component DHF and LL Hamiltonian. See DOI: https://doi.org/10.1039/d2cp05399c

‡ Current address: Department of Chemical Engineering & Materials Science, Michigan State University, East Lansing, Michigan 48824, USA. E-mail: jmendoza@msu.edu

1 Introduction

Our understanding of how chemistry and physical properties evolve across rows and down groups in the modern periodic table has been at the forefront of chemistry for the last 150 years. The latest additions, the so-called actinide elements which are the heaviest elements, are at the frontier of our current chemical and physical understanding.[1–5] The radioactive actinide elements residing underneath the main body of the periodic table conjure images of mushroom clouds, glowing test tubes, and superheroes awakening. While there is some truth to this view, as chemists working beyond the edge of nuclear stability, we have peered into the abyss to find elements whose realities are so complex and mystifying that we do not need to invent fanciful tales to remain a captive audience. Our fundamental knowledge and understanding of actinide bonding trends and coordination modes is significantly limited compared to other elemental series in the periodic table. Even though there are several and thorough studies involving actinide elements,[6–10] there are no studies that use state-of-the-art four-component relativistic methods that permit grasping the contribution of f-type atomic orbitals (AOs) in the electronic structures and chemical bonding of actinides (Ac) to medium-size organic ligands. This is needed to understand the changes in interactions and chemical bonds, which may impact speciation and separation selectivity to different heavy elements.[1–4]

Some chemical reactions can be explained by considering relativistic effects on valence electrons of heavy-atoms, *e.g.* the electromotive force of the cells of lead-batteries, where the relativistic effects on Pb atoms allows for the battery to work.[5] There are also a few other examples which are explained by relativistic effects: *e.g.*, the yellow color of gold, the yellow color of hexachloroplumbate(IV), and the catalytic methane activation by Pt^{+}, to name a few.[11] Based on these grounds, we have undertaken a research program whose goals are oriented to learn more about the physics that underlies the structure and electronic properties of actinide's bonding, where one must consider the influence of relativity. Here we present the first results of our research program, by studying actinide containing compounds with Pu, Am, Cf and Bk and an organic ligand model. Accordingly, we show how the 5f electrons of these actinides behave differently when relativistic effects are taken into account with different theoretical models, thus changing the frontier molecular orbitals of complexes. More specifically, we estimate relativistic effects at the following levels of theory: relativistic zeroth order regular approximation (ZORA) at Hartree–Fock (HF), DFT and DFT-D3 levels;[12,13] four-component (4c) Lévy–Leblond (LL) and 4c-Dirac–Hartree–Fock (DHF).[14] More specifically, (a) the spin–orbit (so) in addition to the scalar (sr) ZORA-DFT and without DFT (ZORA-HF), and (b) 4c-DHF, Lévy–Leblond and spin-free (SF) Hamiltonians.[15] In this manner, it is possible to learn about the influence of both relativistic and electron correlation effects on the geometry, the energy involved in the bonding process and the change of 5f and 6d atomic orbitals (AOs) in the population of molecular orbitals (MOs). To the best of our knowledge, this is the first time that these kinds of large actinide compounds have been studied with highly accurate four-component methods.

The research into carbon-free energy has generated a tremendous interest in alternative energy sources. Nuclear energy is a promising alternative because it offers opportunities for low cost and high efficiency. However, it generates a significant amount of radioactive waste, which we are not able to process or reduce manly because of our lack of understanding of bonding in heavy elements. The appropriate disposal of nuclear waste is still challenging and one of the most difficult kinds of waste to handle because it is highly hazardous and harmful for humans and the biosphere even for small concentrations, and especially if they are radioactive. Advanced actinide separation strategies reduce hazards and costs of managing radioactive waste. Among them liquid fluoride thorium reactor and other molten salt reactor (MSR) have been designed to use the thorium fuel cycle with a fluoride-based, molten, liquid salt for fuel. These reactors are passively safe, produce less radioactive waste, offer higher fuel burn up efficiency, and do not produce industrial quantities of fissile ^{239}Pu.[1] Similarly, the development of vitrification using borate chemistry was inspired, in part, from evidence that a significant boron concentration exists in the brine solutions found at the Waste Isolation Pilot Plant (WIPP) in Carlsbad, New Mexico.[16,17]

Actinide elements are of considerable technological importance, for example in condensed matter, as they may be high temperature superconductors or centers of lasing activity.[3,18] Recently, various studies have been performed in lanthanides and actinide elements to understand the f-orbitals expansion and contractions when loosing or gaining electrons.[3,4,19,20] Therefore, further understanding of the chemical similarities and differences between the trivalent lanthanides and the actinides analogues is of the highest interest. One indication of these advances is the rapid increase in f-block element containing compounds for which high-resolution structures exist, while their properties have been investigated both experimentally and theoretically during the last decade.[2,3] This is promising because the f-electrons remain quite localized in going from the atomic to the condensed state, thus, a lot of knowledge gained from atoms might be transferable to the condensed state.[3,19–21] Therefore, understanding f-block elements and trends is essential, yet challenging because of the intrinsic radioactivity of most of the actinide elements.[4,22] However, this lack of knowledge poses challenges that prevents advances in nuclear energy, radioactive waste management, separation, storage, and next-generation f-electrons materials.[22]

There has been an increasing interest in fundamental research about actinide elements since the 20th century. Understanding the chemical bonding, chemical reactivity, interaction, and speciation of hazardous heavy actinide elements in aqueous solutions are a first step toward modeling their behavior, both in the laboratory and under natural conditions. Although the chemistry of the actinides has been extensively explored for over a century, its theoretical grounds and basic understandings still very much lag behind compared to that of most elements in the periodic table.[23] The ability of actinides to form chemical bonds and the role of 5f and 6d AOs in the contribution to molecular orbitals (MO) are still subjects of investigation.[24,25] We are still developing our

understanding of the role of 5f- and 6d-shell electrons from actinide elements when interacting with other atoms or molecules.

Recently, Silver *et al.* experimentally characterized and synthesized the berkelium coordination complex, Bk(III)tris (dipicolinate), and showed that it had formed a chemically distinct Bk(III) borate material.[26] A recent study has synthesized a nonaqueous isostructural family of f-element compounds (Ce, Nd, Sm, Gd; Am, Bk, Cf) of the redox-active dioxophenoxazine ligand (DOPO = 2,4,6,8-tetra-*tert*-butyl-1-oxo-1*H*-phenoxazin-9-olate) for the first time.[23] Their electronic structure was further studied by applying the zeroth order regular approximation (ZORA) with hybrid DFT as well as CASSCF calculations to predict and investigate the structure, oxidation states, and electronic properties of both the lanthanides and actinides complexes in detail.[23] More recently, Albrecht-Schmitt *et al.* showed that the complexation of berkelium(III) by carbonate results in spontaneous oxidation to berkelium(IV) and that multiple species can be present in solution.[27] They explored the chemistry of Bk(IV) carbonate and carbonate–hydroxide complexes based on theoretical comparisons with spectroscopic data previously reported for Bk(IV) carbonate solutions.[27] They performed molecular orbital calculations to try to obtain a better understanding of the nature of their chemical bonding using DFT at the level B3PW91. Brenner *et al.* synthesized and analyzed the structure, and solid-state UV-vis-NIR spectroscopy of three new f-element squarates, M_2 $(C_4O_4)_3$ $(H_2O)_4$, where M = Eu, Am, Cf and they showed that Cf has a 3^+ ionic state with the nine-coordinate ionic radius of Cf^{3+} about 1.127 ± 0.003 Å.[4] Galley *et al.* synthesized the $Cf(DOPO)_2$ (pyridine)(NO_3) complex and they carried out a computational analysis of the electronic structure of the complex to investigate the ligand-Cf^{III} interactions.[23] Goodwin *et al.* experimentally synthesized an Am^{3+} organometallic complex $[Am(C_5Me_4H)_3]$ and applied DFT and *ab initio* wave function theory calculations to explore the interaction and electronic structure of the complex.[28]

In the next sections we shall first explain the methodology which we have implemented to calculate the geometry and bonding energies of the molecular compounds. We have considered two different levels of theory: (1) ZORA[29–34] and (2) 4c-DHF and LL, with different schemes of basis sets.[32–34] The main idea is to show how important relativistic effects are when one is interested in reproducing those properties and what one can expect when working within the non-relativistic framework. Afterwards we shall focus on one of the main aims of this work, namely, to learn about the dependence of the participation of p-, d- and f-AOs of the actinides atoms on the frontier electronic structure of the just-mentioned family of compounds: Ac-DOPO (Ac = Pu, Am, Cf, Bk) with the above mentioned levels of theory. We shall show that relativistic effects together with electron correlation modify in a great manner the contribution of those AOs, as well as the values of bonding energies.

2 Methods and computational details

All geometrical structures of the Pu-DOPO, Am-DOPO, Cf-DOPO, and Bk-DOPO complexes reported in the present study were fully optimized with different levels of theory: (i) ZORA with hybrid DFT including dispersion corrections, *i.e.*, ZORA-B3LYP-D3 or DFT for short,[24–29] (ii) ZORA-HF, which means ZORA without electron correlation, calculated for only the Am-$DOPO_3$ and Bk-$DOPO_3$ compounds, and (iii) 4c-DHF/LL Hamiltonians with basis sets that are large enough for describing heavy atoms and those in the first coordination sphere to the heavy atoms.[35] The first method essentially improves the usual non-relativistic hybrid DFT[29,30] methods and is useful for general chemistry applications. Long-range van der Waals (vdW) dispersion correction was included.[31] The Grimme's-D3 terms were used for all the light atoms, but due to availability, the dispersion terms from the universal force field (UFF) were employed for actinides. The Slater-Type Orbital (STO) basis sets were used instead of Gaussian-type orbital (GTO) basis sets for the ZORA calculations. Valence triple-ζ with polarization functions (TZP) quality were used for Pu, Am, Cf, and Bk atoms, and the valence double-ζ with polarization functions (DZP) quality STO basis sets were used for the rest of the atoms (C, N, O, and H).[36] In general, the STO basis sets give relatively consistent and rapidly converging results.[37] We have also made ZORA calculations without any DFT functionals.

The second procedure is grounded on the 4c-DHF Hamiltonian, and then its 4c-LL model, to get appropriate non-relativistic (NR) results. In order to compare results obtained with different relativistic methods, though not including in either of them the spin-dependent contributions, we also performed SF calculations to compare them with those of sr-ZORA. All studies were performed by applying a local dense basis set scheme (LDBS),[38] meaning basis sets that are as large as possible for describing the electronic state of heavy atoms, and then, a less complete basis set for atoms that are not much involved in the main fragment of interest (second coordination sphere and beyond). For atoms different to carbon and hydrogen, the selected basis set is dyall-cv3z,[39] while carbon and hydrogen atoms are described with 3-21G Gaussian basis sets.[40,41] Geometries of the complex systems and that of each fragment (actinide atoms and DOPO molecules) were optimized using the DIRAC code.[14] The LDBS scheme was used to describe more accurately the influence of d-shell and f-shell AOs on the bonding of actinide atoms to the oxygen atoms and nitrogen atoms. Only neutral complex systems (*i.e.*, those containing Am and Bk), were considered at the DHF and LL levels of theory because it is not feasible to achieve the geometry optimization of open-shell systems with an analytical gradient in the current implementation of the DIRAC code.

On the other hand, to calculate the bonding energies (BEs) at DHF and LL levels of approach, we calculated the electronic energy of the complex system by including at the beginning of the calculation a higher density of charges on the nitrogen atoms (−1 each) and a lower charge density on the Ac atoms (+3). Then we optimized the geometry of the fragments as closed-shell systems though ionized, meaning Ac^{+3} and $DOPO^{-1}$, and taking then their electronic energy. We have also calculated the energy of the neutral DOPO structure (which is an open-shell system) by making a single-point calculation with

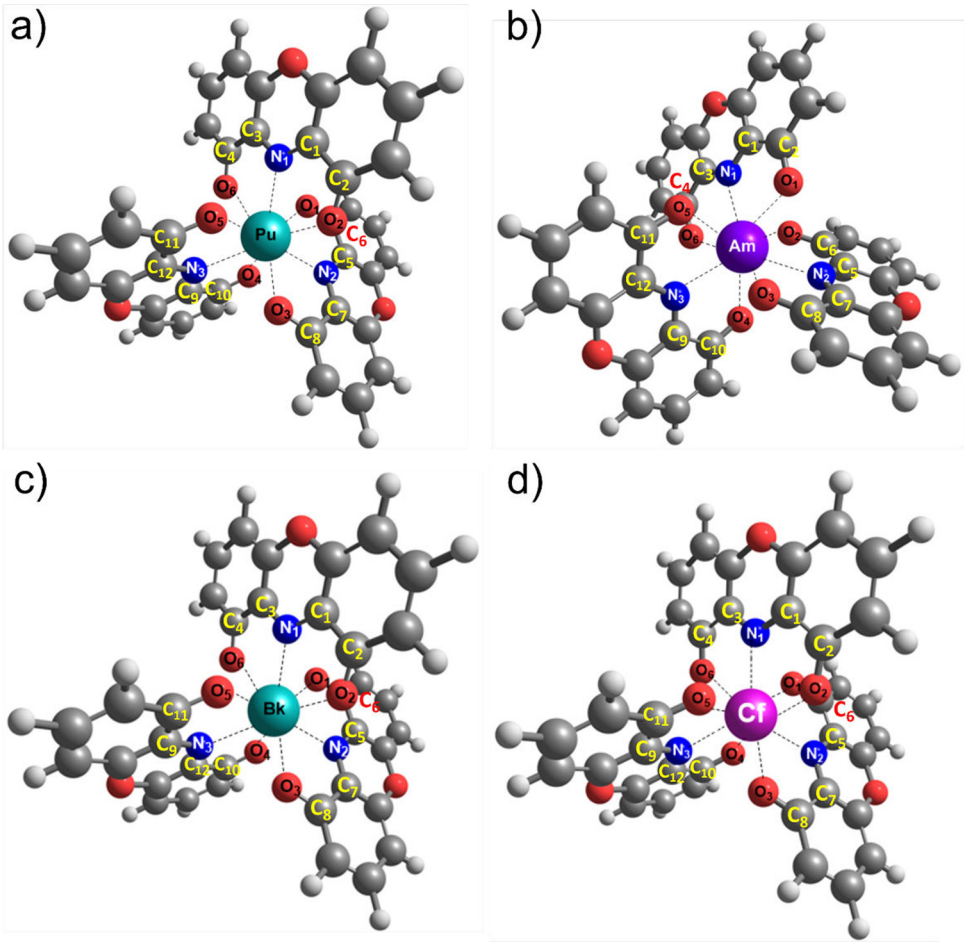

Fig. 1 Optimized structures of Ac-DOPO compounds with (a) Ac = Pu, (b) Ac = Am, (c) Ac = Bk, and (d) Ac = Cf.

the geometry of the ionized DOPO fragment. The energies of the actinides were also obtained from a single-point calculation with the DIRAC code at the DHF and LL levels of theory. On the other hand, the BEs of both actinides systems, Am-$DOPO_3$ and Bk-$DOPO_3$ were calculated at the ZORA level of approach without any restriction (results of calculations with close-shell configurations and the open-shell configurations are shown in the ESI†).

The whole set of model compounds considered in this work has been experimentally synthesized and characterized, and denoted as Ac-DOPO (Fig. 1). In all computations no constraints were imposed on the geometry. The sr-ZORA-DFT calculations in addition to the so-ZORA-HF calculations were performed with the Amsterdam density functional (ADF) code[42] while the 4c-DHF, 4c-LL and 4c-DHF-SF calculations were performed with the Dirac code.[14] The ADF-GUI[42] program was used for visualization of the highest occupied molecular orbitals (HOMO) and lowest unoccupied molecular orbitals (LUMO) from the ZORA-DFT calculations. The ligand field diagram (LFD) analysis of the Ac-$DOPO_3$ system (Ac = Pu, Am, Cf and Bk) for all actinides was performed using the ZORA approximation, while DHF and LL levels of theory were used only for Am and Bk. In addition we mention that the timings for both ADF and DIRAC calculations are few orders of magnitude different (around two orders), but still the timing of the calculations at the 4c level of theory is of the order of 100 hours. As an example, the time of the SCF calculation for Ac(III). $3DOPO^{-1}$ at the 4c-B3LYP/(Am, O, N: cv3z, C, H: 3-21G) level of theory with 16 processors and 8 GB of RAM/proccesor was of 53 hours.

In Tables S10–S16 of the ESI† file we give the bonding energies of the Am-$DOPO_3$ and Bk-$DOPO_3$ complexes considering both ionized and neutral fragments.

3 Results and discussion

We shall first show the influence of relativistic effects on the geometric parameters of the actinide compounds, and then on BEs. Afterwards, we shall show how important the contributions of each of the valence-shell p-, d- and f-AOs of actinides are in the electronic framework of the frontier MOs, HOMO–LUMO.

3.1 Geometrical structures

The optimized geometry of a Pu-$DOPO_3$ complex at the ZORA level is shown in Fig. 1a. The root mean square deviation

(RMSD) value of all the 1st coordination bonds (Pu–N, Pu–O) w.r.t. to experiments is 0.104 Å, while the RMSD for the 2nd coordination sphere (C–C, C–N, and C–O) is 0.046 Å, as shown in Tables S1–S3 (ESI†). In other words, the calculations at the ZORA-DFT-D3 level of approach estimate the experimental Pu–N and Pu–O bonds to 0.1 Å of error, which is the order of magnitude for high quality X-ray structures.

The optimized geometry of the Am-DOPO complex is shown in Fig. 1b. In this case, we used four different levels of theory: ZORA-HF, ZORA-DFT, ZORA-DFT-D3, 4c-LL and 4c-DHF (see Table 1 and Table S4, ESI†). The RMSD for the bond lengths of Am–N_1 and Am–O_1 are 0.206, 0.024, 0.052, 0.023, 0.050 (in Å) and 0.149, 0.120, 0.106, 0.103, 0.066 (in Å), respectively. This trend is in agreement with the increasing accuracy of the level of theory, with 4c-DHF showing the highest values of RMSD, and the smallest is found for d(Am–O_1) though there are very small values of RMSD for d(Am–N_1). In this last case only at the ZORA-HF level did we obtain RMSD values that are larger than 0.1 Å. The results of 4c-DHF-SF calculations give the same bond lengths as those of ZORA-DFT. Looking more closely at the bonds, the calculations with ZORA-DFT-D3 are within a difference of 0.105 Å for Am–O_1 and 0.046 Å for Am–N_1 (Table S5, ESI†). When they are calculated with the Lévy–Leblond model, those differences are 0.102 Å and 0.029 Å, respectively. In the case of DHF calculations these differences are within 0.066 Å and 0.054 Å, respectively. This means that both electron correlation and relativistic effects must be included to best reproduce experimental measurements, though relativistic effects showed by DHF calculations give the best reproduction of d(Am–N_1) and d(Am–O_1). Remarkably, ZORA with dispersion corrections improves the RMSD only a bit *versus* calculations without it.

All this analysis suggests that dispersion corrections might not be necessary to consider for this type of compounds, as they were not included in the 4c-LL and 4c-DHF calculations either. Considering that electron correlation effects can be obtained as the difference between ZORA-DFT and ZORA-HF calculations, we found that these effects increase both distances: in average 0.166 Å for d(Am–N_1) and 0.267 Å for d(Am–O_1). On the other hand, considering that relativistic effects can be obtained as the difference between DHF and LL calculations we found that they increase the values of d(Am–N_1) (0.024 Å in average) but diminish that of d(Am–O_1) (0.037 Å in average) though in a much smaller amount as compared with the influence of those distances by the electron correlation effects.

The geometry of the Bk-DOPO complex was calculated with the three levels of theory mentioned above. In Fig. 1c we show its equilibrium geometry. The bond distances Bk–N and Bk–O at equilibrium and for all methods used here are collected in Table 2. The RMSD is 0.082, 0.114 and 0.063 for ZORA-DF-D3, 4c-LL and 4c-DHF, respectively. The distances at the 4c-DHF level of theory give again the smallest value of RMSD, which one might expect since it is the most accurate. Similarly to what happens with Ac = Am, the bond lengths with 4c-DHF have the same consistent sign, though calculations at ZORA and 4c-LL levels underestimate the Bk–N bonds. Once both effects, electron correlation and relativistic effects are introduced, the behavior of those bond distances follows a similar trend as observed for Am. In this case, electron correlation effects are quite similar to those of the relativistic effects for d(Bk–N).

The last system studied was Cf-DOPO for which the oxidation state is +3. Its equilibrium structure is shown in Fig. 1d. The bond distances at equilibrium, Cf–N and Cf–O, are collected in Table S6 (ESI†). There are no experimental or previous theoretical results for comparison of Cf complexes. Our calculations at the ZORA-DFT-D3 level of theory shows that the average Cf–N bond distance is slightly higher than the average Pu–N bond distance by 0.037 Å, and similarly the average Cf–O bond distance is slightly higher than the average Pu–O bond distance by 0.083 Å. The average bond distances for Cf–N and Cf–O are reported in Table S7 (ESI†), where, as happens with Am, the introduction of dispersion correction to the ZORA calculations changes the bond length slightly.

3.2 Bonding energies

For these calculations we shall consider the Am and Bk containing systems as model compounds. The bonding energies (BE) are calculated, at all levels of approach, as: BE = Ac[DOPO]$_3$ − (Ac(III) + 3DOPO^{-1}).

Table 1 The equilibrium bond distances of Am–N_1 and Am–O_1 at different levels of theory. All values are given in Å

	Bond length						Difference w.r.t. experiments				
Bonds	Expt.[a]	ZORA-HF	ZORA-DFT	ZORA-DFT-D3	4c-LL	4c-DHF	ZORA-HF	ZORA-DFT	ZORA-DFT-D3	4c-LL	4c-DHF
Am–N_1	2.591	2.372	2.554	2.542	2.614	2.626	−0.219	−0.037	0.049	−0.023	−0.035
Am–N_2	2.582	2.369	2.563	2.522	2.601	2.621	−0.213	−0.019	0.060	0.019	0.039
Am–N_3	2.554	2.369	2.546	2.507	2.581	2.623	−0.185	−0.008	−0.047	0.027	0.069
RMSD							0.206	0.024	0.052	0.023	0.050
Am–O_1	2.472	2.334	2.592	2.595	2.588	2.541	−0.138	0.120	0.123	0.116	0.069
Am–O_2	2.465	2.321	2.614	2.573	2.571	2.536	−0.144	0.149	0.108	0.106	0.071
Am–O_3	2.476	2.314	2.557	2.558	2.556	2.538	−0.162	0.081	0.082	0.080	0.062
Am–O_4	2.462	2.333	2.579	2.579	2.580	2.545	−0.129	0.117	0.117	0.118	0.083
Am–O_5	2.481	2.324	2.621	2.586	2.581	2.539	−0.157	0.140	0.105	0.100	0.058
Am–O_6	2.493	2.332	2.592	2.586	2.583	2.544	−0.161	0.099	0.093	0.090	0.051
RMSD							0.149	0.12	0.106	0.103	0.066

[a] Taken from ref. 3.

Table 2 The equilibrium bond distances Bk–N and Bk–O in the Bk-DOPO complex. All values are given in Å

	Bond length					Difference w.r.t. experiments			
Bonds	Expt.[a]	ZORA-HF	ZORA-DFT-D3	4c-LL	DHF	ZORA-HF	ZORA-DFT-D3	4c-LL	DHF
Bk–N_1	2.521	2.338	2.494	2.547	2.585	0.183	−0.027	0.026	0.064
Bk–N_2	2.571	2.406	2.441	2.432	2.584	0.165	−0.130	−0.139	−0.013
Bk–N_3	2.544	2.354	2.492	2.486	2.587	0.178	−0.040	−0.046	0.055
RMSD						0.175	0.080	0.086	0.049
Bk–O_1	2.459	2.346	2.59	2.579	2.478	0.114	0.130	0.119	0.018
Bk–O_2	2.436	2.320	2.495	2.592	2.509	0.126	0.049	0.146	0.063
Bk–O_3	2.454	2.336	2.505	2.569	2.492	0.117	0.052	0.116	0.039
Bk–O_4	2.468	2.323	2.583	2.569	2.529	0.145	0.115	0.101	0.061
Bk–O_5	2.447	2.329	2.532	2.555	2.534	0.118	0.085	0.108	0.087
Bk–O_6	2.452	2.313	2.528	2.626	2.549	0.139	0.076	0.174	0.097
RMSD						0.127	0.090	0.130	0.066

[a] Taken from ref. 3.

As shown in Table 3, we have performed calculations at four-component levels in such a way that we are able to analyze the influence of relativistic effects (DHF-LL), SO effects at the DHF level of approach (DHF – DHF – SF) and electron correlation (4c-B3LYP-DHF). We have also performed calculations at the ZORA level of theory and there we can analyze the influence of SO effects and the electron correlation. Given that we include calculations that consider the actinide atom with different multiplicities we are able to learn about what kinds of calculations give results that are closer to the four-component ones.

The behavior of relativistic effects is opposite for Am-$(DOPO)_3$ and Bk-$(DOPO)_3$ complexes. For the first actinide relativistic effects on BE are positive (0.139 au) of which SO effects are the most important (0.105 au). In contrast, the berkelium relativistic effects on BE are of opposite sign (−0.319 au) and in this case the SO effect is smaller (−0.083 au) when it is compared with its equivalent in Am.

On the other hand, at the sr-ZORA level of approach we found that BEs are much dependent on the multiplicity of the actinide atom. One should compare results of DHF-SF calculations with that of sr-ZORA/HF. For both actinides the more approximated results of ZORA calculations are found for the quintuplet multiplicity. Besides, given that the so-ZORA calculations are performed with the closed-shell system its results must be comparable with that of DHF.

When electron correlation is considered at each of both levels of theory we found different behaviors. At the ZORA level the electron correlation for Am is equal to: −2.128 au + 1.335 au =

Table 3 Bonding energies (BE) for Am and Bk, calculated at the DHF, DHF-spin-free (DHF-SF), Lévy–Leblond (LL) and sr (so)-ZORA levels of approach, expressed in a.u. (between parentheses in kJ mol^{-1})

	$Am(III)\cdot 3DOPO^{-1}$	$Am(III)$	$DOPO^{-1}$	BE[a]	ΔE^b
DHF	−32 694.990	−30 488.849	−734.889	−1.475 (−3872.613)	−0.054 (140.727)
DHF-SF	−32 619.097	−30 412.630	−734.929	−1.680 (−4410.840)	
4c-LL	−29 897.818	−27 692.640	−734.521	−1.614 (−4237.557)	−0.088 (−230.519)
4c-B3LYP	−32 722.070	−30 503.042	−738.977	−2.097 (−5505.674)	
so-ZORA/HF	−32.023	−0.056	−10.211	−1.335 (−3505.043)	
sr-ZORA/HF[c]	−31.835	1.229	−10.211	−2.432 (−6385.216)	
sr-ZORA/HF[d]	−31.474	0.569	−10.211	−1.411 (−3704.581)	
sr-ZORA/B3LYP[c]	−20.814	1.457	−6.609	−2.445 (−6419.348)	
sr-ZORA/B3LYP[d]	−20.756	1.296	−6.609	−2.226 (−5844.363)	
sr-ZORA/B3LYP[e]	−20.593	1.096	−6.609	−1.863 (−4891.307)	
so-ZORA/B3LYP	−20.997	1.001	−6.609	−2.128 (−5587.064)	
	$Bk(III)\cdot 3DOPO^{-1}$	$Bk(III)$	$DOPO^{-1}$	BE[a]	ΔE^b
DHF	−34 397.417	−32 190.967	−734.889	−1.784 (−4683.717)	−0.060 (−157.530)
DHF-SF	−34 308.076	−32 101.587	−734.929	−1.701 (−4466.633)	
4c-LL	−31 301.618	−29 096.589	−734.521	−1.465 (−3846.620)	−0.105 (−275.677)
4c-B3LYP	−34 425.524	−32 206.471	−738.977	−2.121 (−5569.274)	
so-ZORA/HF	−32.172	0.310	−10.211	−1.850 (−4856.272)	
sr-ZORA/HF[c]	−31.916	1.377	−10.211	−2.661 (−6986.276)	
sr-ZORA/HF[d]	−31.707	0.780	−10.211	−1.855 (−4870.303)	
sr-ZORA/B3LYP[c]	−20.846	1.562	−6.609	−2.581 (−6776.416)	
sr-ZORA/B3LYP[d]	−20.804	1.390	−6.609	−2.367 (−6214.559)	
sr-ZORA/B3LYP[e]	−20.624	1.176	−6.609	−1.974 (−5182.737)	
so-ZORA/B3LYP	−21.004	1.185	−6.609	−2.362 (−6201.431)	

[a] At DHF and LL levels of approach: $BE = Ac[DOPO]_3 - (Ac(III) + 3DOPO^{-1})$. [b] $\Delta E = E$(DHF with optimized ZORA geometry) − E(DHF with optimized DHF geometry) or E(LL with ZORA geometry) − E(LL with LL optimized geometry), respectively. [c] Singlet multiplicity. [d] Quintuplet multiplicity. [e] Septuplet multiplicity.

−0.793 au. For Bk it is −2362 au + 1.850 au = −0.712 au. In the case of 4c calculations, for Am the electron correlation is: −2.097 au + 1.475 au = −0.622 au which is close to that of ZORA. But in the case of Bk the electron correlation is: −2.121 au + 1.784 au = −0.337 au which is almost half that of the ZORA calculation.

Furthermore one may assume that when electron correlation effects are included at the 4c-B3LYP level of theory their results must be close to those of so-ZORA/B3LYP calculations. In the case of the Am-DOPO compound this is what we found: −2.097 au *vs.* −2.128 au (−5505.67 kJ mol^{-1} *vs.* −5587.06 kJ mol^{-1}) but for the Bk-DOPO compound a little large difference appears: −2.121 au *vs.* −2.362 au (−5568.69 kJ mol^{-1} *vs.* −6201.43 kJ mol^{-1}). We are aware that both methodologies, ZORA/B3LYP and 4c/B3LYP, have different grounds. The first one uses a frozen core description of the electronic behavior but the other is an all electron methodology.

We could shed some more light on the reason why those differences arise by observing the energy-spectra of the frontier orbitals shown in Fig. 2 for the Am-$(DOPO)_3$ complex. We show the energy of MOs that belongs to HOMO–LUMO structures of sr-ZORA/B3LYP, 4c/B3LYP and 4c-DHF. There is a clear difference among the energy-gap between HOMO–LUMO orbitals and also the influence of f-type AOs in them.

Another finding is that by including electron correlation both molecular systems become more stable.

Our previous analysis shows that higher levels of theory, such as DHF, might be needed to obtain a better estimation not only of the geometry but also a more accurate estimation of reaction energies (see Table 3). Additionally, the basis set superposition error is less than 6% for the BE of both, Am-$(DOPO)_3$ and Bk-$(DOPO)_3$ complexes.

3.3 Influence of p-, d- and f- AOs on the HOMO–LUMO electronic structure

After obtaining the optimized structures of the Pu-$(DOPO)_3$, Am-$(DOPO)_3$, Cf-$(DOPO)_3$ and Bk-$(DOPO)_3$ complexes, we further carried out an investigation of the contribution of the valence AOs of the heavy elements (Pu, Am, Cf, and Bk) to the frontier MOs by analyzing the pattern of the HOMO–LUMO electronic structure and the LFD diagram. We achieved reliable results for both, Am-$DOPO_3$ and Bk-$DOPO_3$ compounds at the 4c level of approach (Tables S8 and S9, ESI†). The other complex systems (those for which Ac = Pt, Cf) are not closed-shell and so they cannot be studied with the current version of the DIRAC code. On the other hand, the Lévy–Leblond calculation of the structure of frontier orbitals of Bk-$(DOPO)_3$ is not as reliable for Am-$(DOPO)_3$. In this last case the HOMO–LUMO orbitals of Bk-$(DOPO)_3$ have some inconsistencies in the LUMO structure, likely arising from linear dependence.

To further understand the bonding structure of the electronic framework in the Am$(DOPO)_3$ complex, LFD computations were first performed at the ZORA level (Fig. 2). This calculation shows that the 5f-AOs of Am and DOPO ligands are taking part to create MOs with a bonding character. The HOMO and LUMO orbitals in which those AOs are more involved are HOMO−9, HOMO−11, LUMO+3 and LUMO+6 (Fig. S6 and S7, ESI†). The study of 5f- and 5p-AOs of Am contributions to frontier MOs was also performed at both DHF and LL levels of theory to corroborate the previous findings at the ZORA level. There are significant contributions of Am 5f- and 6p-AOs to HOMO−6 (fxyy = 0.271, fxxy = 0.271, fxxx = 0.091) and LUMO+3 (py = 0.633, px = 0.241, pz = 0.043) molecular orbitals (Table S9, ESI†). Thus, we found a similar scheme to that of ZORA-DFT-D3 though with little differences (see Fig. 2). It is important to point out that those relativistic effects are largely involved. At the LL level of theory, the contribution of 5f-AO of Am to HOMO−6 is lost, and there is no significant contribution of them to any HOMO−n (n = 1–12). On the other hand, the pattern of the 5f-AOs contributions to LUMO+n orbitals (n = 9) are just slightly modified, *e.g.*, LUMO+3 (py = 0.587, px = 0.234, pz = 0.043). Thus, without the relativistic approximations (the LL reference method), there are no contributions to the HOMO−n orbitals, which are present when ZORA or DHF are used. This is a remarkable finding because it implies that relativistic effects play a central role in the involvement of f-orbitals in the frontier orbitals. Intuitively, this is an expected result due to the well-known influence of direct/indirect relativistic effects on the size of AOs, which means the contraction/expansion of the p-AOs/f-AOs. This is now numerically observed on these actinide compounds. Furthermore, the pattern of energies of the set of HOMO−n (n= 1–8) orbitals at both the four-component and NR level of theory are quite similar.

A similar interaction symmetry can be seen in LUMO+4 and LUMO+5.

The analysis of the contributions from Bk 5f-AOs to the frontier MOs was also performed at the LL and DHF level of

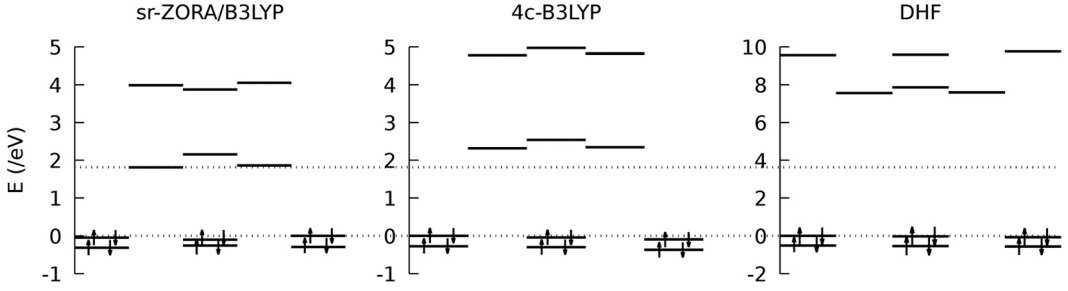

Fig. 2 Ligand Field Diagram (LFD) of the Am-DOPO system calculated at the sr-ZORA/B3LYP, 4c-B3LYP and 4c-DHF levels of theory. Each energy-level was scaled with respect to the energy of the HOMO.

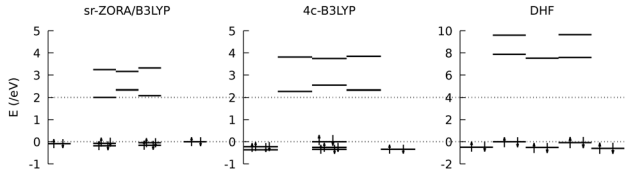

Fig. 3 Ligand Field Diagram (LFD) of the Bk-DOPO system calculated at the sr-ZORA/B3LYP, 4c-B3LYP and 4c-DHF levels of theory. Each energy-level was scaled with respect to the energy of the HOMO.

theory for comparison with ZORA calculations. There are significant contributions of Bk 5f- and 6p-AOs to HOMO−8 (fxyy = 0.171, fxxy = 0.114, fxxx = 0.063) and LUMO+3 (py = 0.578, px = 0.268, fxyy = 0.054) molecular orbitals at the DHF level (Table S10, ESI†). The non-relativistic calculations were performed with LL Hamiltonian, but in this case some inconsistencies appears because the LUMO and LUMO+1 orbital energies are negative (see Table S9 in ESI†), and few linear dependencies arise in the wave function calculation. In summary, as was also observed for the complexed Am compound the symmetry, magnitude and types of Bk-AOs are affected by relativistic effects, which in turn will affect how we interpret bonding and reaction on these compounds. This calls for caution when interpreting standard DFT calculations without scalar or 4-component relativistic effects for bonding or reactions.

First, we focus on the Pu AOs involved in the bonding. The LFD of the Pu-$(DOPO)_3$ complex shows that the electronic 5f-orbitals of plutonium are interacting with the 2p-orbitals of both the N and O atoms (Fig. S3, ESI†). To provide further insight about the interaction between Pu and N or O atoms, we have computed the HOMO–LUMO and HOMO−n and LUMO+n MOs (Fig. S4 and S5, ESI†). These diagrams shows that the Pu AOs interact with the DOPO ligand AOs to create molecular orbitals with a bonding character. To give an example, three of the highest bonding molecular orbitals, HOMO, HOMO−6 and HOMO−9 show that 5f-orbital electrons of plutonium interact with the 2p-AOs of the N, O and even C atoms. More specifically in the HOMO, the 5f-AO is delocalized with a 2p AO from N atom in the organic ligand (Fig. S4, ESI†). Similarly, we can observe in LUMO, LUMO+1, LUMO+2 and LUMO+6 that the Pu 5f-AOs are delocalized with the 2p-AO from N and O atoms, but not C, in the ligand (Fig. S5, ESI†). This is evidence that at the ZORA level of theory the 5f-AOs of the Pu play an important role in creating a bond with the organic ligand, *i.e.*, 5f-AOs are crucial to describe the bonding of the $Pu(DOPO)_3$ complex.

The bonding interactions between Cf and DOPO (Fig. S8, ESI†) were studied by analyzing the LFD of Cf-$(DOPO)_3$. The LFD shows that near the frontier orbitals, the 5f-AOs of Cf interact with the N, O and even with the C atoms in the HOMO orbitals. However only C and N participate in the LUMO near the frontier. The HOMO and LUMO orbitals were calculated at the ZORA level of theory (Fig. S9 and S10, ESI†). In HOMO−7, HOMO−8 and HOMO−10, the overlap between 5f-AOs and AOs from the ligand can be observed, which have some bonding character. A similar study was performed on Bk containing compounds. The LFD shows that 5f-AOs of Bk are interacting with the carbon atom in the DOPO ligand of the complex (Fig. 3 and Fig. S11, ESI†), which is also observed qualitatively in the HOMO–LUMO representations at the ZORA level (Fig. S12 and 13, ESI†). The overlap of the 5f-AOs can be seen in HOMO−7, HOMO−8 and HOMO−9.

4 Conclusions

We computationally investigated the molecular structure at equilibrium of the f-block element (Pu, Am, Bk, and Cf) compounds of the redox-active DOPO ligand by using (i) four-component with Dirac–Hartree–Fock (DHF), Lévy–Leblond (LL) and spin-free (SF) Hamiltonians, together with (ii) the scalar relativistic (sr) and spin–orbit relativistic (so) zeroth-order regular approximation (ZORA) with hybrid density functional theory (DFT).

We found that the RMSD values for bond distances are the smallest when the DHF method is applied, followed by the results of calculations with the ZORA and LL levels of theory. Taking both Ac-DOPO (Ac = Am, Bk) compounds as model compounds, we found that relativistic effects shorten the bond distances on average by 0.04 Å for Am–O_1 and 0.07 Å for Bk–O. Furthermore, all six Am–O_1 bond distances and the three Am–N_1 bond distances become closer to each other when four-component relativistic effects are included, and they are also closer to experimental distances as compared with the sr-ZORA results. Total relativistic effects shortened the Ac–Obond distances but expanded the Ac–N bond distances. When considering the scalar relativistic effects, we found that they shorten Ac–N bond lengths but the spin-dependent relativistic effects expand them. The opposite behavior is found for the Ac–O bond lengths. Furthermore, electron correlation stretches the bond distances of Ac–N and Ac–O though the effect on stretching the distance d(Ac–O) is larger than that effect on d(Ac–N).

On the other hand, we found that the BE is more negative when it is calculated at the 4c-DHF level of theory than for the so-ZORA/HF level of theory for the Am-$DOPO_3$ complex (-3872.61 kJ mol^{-1} *vs.* -3505.04 kJ mol^{-1}, respectively). For the Bk-$DOPO_3$ complex this tendency is opposite (-4683.89 kJ mol^{-1} *vs.* -4857.20 kJ mol^{-1}, respectively). In both cases the inclusion of electron correlation at any level of theory makes those systems more stable. This illustrates that working with more accurate levels of theory, such as the one that considers four-component Hamiltonians and all-electron calculations, might be needed to obtain a better estimation of the geometrical structure and even a more accurate estimation of reaction energies for Ac-$DOPO_3$ complexes.

We have also analyzed the contributions of 5f- and 6p-AOs of central actinides (Ac = Am, Bk) to frontier MOs at both levels of theory, ZORA and DHF. We found that for Ac = Am, there are significant contributions of Am 5f- and 6p-AOs to the HOMO−6 (fxyy = 0.271, fxxy = 0.271, and fxxx = 0.091) and LUMO+3 (py = 0.633, px = 0.241, and pz = 0.043). However, with the non-relativistic LL Hamiltonian the Am 5f-AO contribution to HOMO−6 is lost and also any other HOMO−n (n = 1–12). This

means that, without including relativistic effects at the ZORA or DHF level, no contributions of the Am 5f-AOs to the HOMO−*n* orbitals are found. This shows that relativistic effects play a key role in the population of f-orbitals in the frontier orbitals. A similar behavior occurs for the Bk-containing compound, where the symmetry and the magnitude of Bk-AOs are also affected by relativistic effects. In this case the HOMO−8 (fxyy = 0.171, fxxy = 0.114, fxxx = 0.063) and LUMO+3 (py = 0.578, px = 0.268, pz = 0.054) have Bk-AO contributions.

We can state now that calculations at both ZORA and DHF (with a given local dense basis set) levels of approach give good estimation of geometries, which can be useful when the experimental synthesis is challenging or not cost-effective, and also that the reaction of these complexes can only be adequately reproduced if they are described within a relativistic framework, given that the change depends on the frontier MOs. This is a call for caution for using standard DFT calculations when the complex studied involves actinide elements. One must include either, scalar or four-component relativistic effects on the calculations of bonding and reactions. In addition, we want to emphasize that one must include an adequate local dense basis set scheme for making the results of calculations at the DHF level reliable.

As a continuation of our line of research and based on these results, we started the study of some response properties like the NMR spectroscopic parameters, which shall provide new insights about the physics behind these Actinide-containing systems.

Conflicts of interest

There are no conflicts to declare.

Acknowledgements

G. A. A. acknowledge support from the Argentinian National Founding for Science and Technique, FONCYT (Grant PICT2016-2936). S. P. thanks the Science and Engineering Research Board, Department of Science and Technology (SERB-DST), Govt. of India for providing the Ramanujan Faculty Fellowship under the scheme no. SB/S2/RJN-067/2017 and the Early Career Research Award (ECRA) under the project number ECR/2018/000255. The computing for this project was performed partly on the High-Performance Computer cluster at the Research Computing Center at Florida State University (FSU). A large portion of this work was supported in part through computational resources and services provided by the Institute for Cyber-Enabled Research at Michigan State University (MSU).

Notes and references

1 Y. Ohtsuka, M. Aoyama, Y. Takaku, Y. Igarashi, M. Hattori, K. Hirose and S. Hisamatsu, *Sci. Rep.*, 2019, **9**, 1–8.
2 N. Greenwood and A. Earnshaw, *Chemistry of the Elements*, Butterworth-Heinemann, 2nd edn, 1997.
3 S. S. Galley, S. A. Pattenaude, C. A. Gaggioli, Y. Qiao, J. M. Sperling, M. Zeller, S. Pakhira, J. L. Mendoza-Cortes, E. J. Schelter and T. E. Albrecht-Schmitt, *et al.*, *J. Am. Chem. Soc.*, 2019, **141**, 2356–2366.
4 N. Brenner, J. M. Sperling, T. N. Poe, C. Celis-Barros, K. Brittain, E. M. Villa, T. E. Albrecht-Schmitt and M. J. Polinski, *Inorganic Chem.*, 2020, **59**, 9384–9395.
5 A. Leszczyk, P. Tecmer and K. Boguslawski, *Transition Metals in Coordination Environments*, Springer, 2019, pp. 121–160.
6 W. H. E. Schwarz, E. M. van Wezenbeek, E. J. Baerends and J. G. Snijders, *J. Phys. B: At., Mol. Opt. Phys.*, 1989, **22**, 1515–1530.
7 M. Pepper and B. E. Bursten, *Chem. Rev.*, 1991, **91**, 719–741.
8 M. Dolg and X. Cao, *Recent Advances in Relativistic Molecular Theory*, World Scientific, 2004, vol. 5, pp. 1–36.
9 L. A. Seaman, G. Wu, N. Edelstein, W. W. Lukens, N. Magnani and T. W. Hayton, *J. Am. Chem. Soc.*, 2012, **134**, 4931–4940.
10 M. P. Kelley, J. Su, M. Urban, M. Luckey, E. R. Batista, P. Yang and J. C. Shafer, *J. Am. Chem. Soc.*, 2017, **139**, 9901–9908.
11 P. Pyykkö, *Annual Rev. Phys. Chem.*, 2012, **63**, 45–64.
12 C. Chang, M. Pelissier and P. Durand, *Phys. Scr.*, 1986, **34**, 394.
13 E. van Lenthe, E.-J. Baerends and J. G. Snijders, *J. Chem. Phys.*, 1994, **101**, 9783–9792.
14 A. S. P. Gomes, T. Saue, L. Visscher, H. J. A. Jensen, R. Bast, V. Bakken, K. G. Dyall, S. Dubillard, U. Ekström and E. Eliav *et al.*, *DIRAC, a relativistic ab initio electronic structure program*, 2019.
15 T. Saue, *Chem. Phys. Chem.*, 2011, **12**, 3077–3094.
16 A. Goel, J. S. McCloy, R. Pokorny and A. A. Kruger, *J. Non-Cryst. Sol.: X*, 2019, **4**, 10033.
17 J. D. Vienna, *Int. J. Applied Glass Sci.*, 2010, **1**, 309–321.
18 Z. Fisk, D. Hess, C. Pethick, D. Pines, J. Smith, J. Thompson and J. Willis, *Science*, 1988, **239**, 33–42.
19 M. van Schilfgaarde, I. Abrikosov and B. Johansson, *Nature*, 1999, **400**, 46–49.
20 A. M. Boring and J. L. Smith, *Los Alamos Sci.*, 2000, **26**, 90.
21 C. Cao, R. E. Vernon, W. Schwarz and J. Li, *Front. Chem.*, 2021, **8**, 813.
22 N. G. Cooper, *Los Alamos Sci.*, 2000, **26**, 1–493.
23 S. S. Galley, C. A. Gaggioli, M. Zeller, C. Celis-Barros, T. E. Albrecht-Schmitt, L. Gagliardi and S. C. Bart, *Chem. – Eur. J.*, 2020, **26**, 8885–8888.
24 M. Tobisu, H. Kinuta, Y. Kita, E. Remond and N. Chatani, *J. Am. Chem. Soc.*, 2012, **134**, 115–118.
25 S. Kundu, Y. Choliy, G. Zhuo, R. Ahuja, T. J. Emge, R. Warmuth, M. Brookhart, K. Krogh-Jespersen and A. S. Goldman, *Organometallics*, 2009, **28**, 5432–5444.
26 M. A. Silver, S. K. Cary, J. A. Johnson, R. E. Baumbach, A. A. Arico, M. Luckey, M. Urban, J. C. Wang, M. J. Polinski and A. Chemey, *et al.*, *Science*, 2016, **353**, aaf3762.

27 T. E. Albrecht-Schmitt, D. E. Hobart, D. Páez-Hernández and C. Celis-Barros, *Int. J. Quantum Chem.*, 2020, **120**, e26254.
28 C. A. Goodwin, J. Su, T. E. Albrecht-Schmitt, A. V. Blake, E. R. Batista, S. R. Daly, S. Dehnen, W. J. Evans, A. J. Gaunt and S. A. Kozimor, *et al.*, *Angew. Chem., Int. Ed.*, 2019, **58**, 11924.
29 A. D. Becke, *J. Chem. Phys.*, 1993, **98**, 5648–5652.
30 C. Lee, W. Yang and R. G. Parr, *Phys. Rev. B: Condens. Matter Mater. Phys.*, 1988, **37**, 785.
31 S. Grimme, *J. Comput. Chem.*, 2006, **27**, 1787–1799.
32 E. van Lenthe, E.-J. Baerends and J. G. Snijders, *J. Chem. Phys.*, 1993, **99**, 4597–4610.
33 E. van Lenthe, R. Van Leeuwen, E.-J. Baerends and J. G. Snijders, *Int. J. Quantum Chem.*, 1996, **57**, 281–293.
34 E. v Van Lenthe, J. Snijders and E. Baerends, *J. Chem. Phys.*, 1996, **105**, 6505–6516.
35 D. Cremer, W. Zou and M. Filatov, *Wiley Interdiscip. Rev.: Comput. Mol. Sci.*, 2014, **4**, 436–467.
36 E. Van Lenthe and E. J. Baerends, *J. Comput. Chem.*, 2003, **24**, 1142–1156.
37 M. Guell, J. M. Luis, M. Sola and M. Swart, *J. Phys. Chem. A*, 2008, **112**, 6384–6391.
38 K. G. Dyall, *Theor. Chem. Acc.*, 2007, **117**, 491–500.
39 K. G. Dyall, *Theor. Chem. Acc.*, 2012, **131**, 1–11.
40 J. S. Binkley, J. A. Pople and W. J. Hehre, *J. Am. Chem. Soc.*, 1980, **102**, 939–947.
41 M. S. Gordon, J. S. Binkley, J. A. Pople, W. J. Pietro and W. J. Hehre, *J. Am. Chem. Soc.*, 1982, **104**, 2797–2803.
42 G. te Velde, F. M. Bickelhaupt, E. J. Baerends, C. Fonseca Guerra, S. J. A. van Gisbergen, J. G. Snijders and T. Ziegler, *J. Comput. Chem.*, 2001, **22**, 931–967.